Tomographic characterization of OPO sources close to threshold

Virginia D'Auria[a,b], Antonino Chiummo[a,b], Martina De Laurentis[b], Alberto Porzio[a], and Salvatore Solimeno[a,b]

[a]Coherentia – INFM and [b]Dipartimento di Scienze Fisiche Univ. "Federico II", Compl. Univ. MSA, Via Cintia, I–80126, Napoli, Italy

name.surname@na.infn.it

Matteo G.A. Paris

INFM and Dipartimento di Fisica, Universita' degli studi di Milano, Italia, via Celoria 16 I-20133, Milano, Italy

Abstract: Pattern function quantum homodyne tomography (QHT) has been used for characterizing the ouput of a degenerate below–threshold type–I OPO. The recovered photon number distributions deviated from those relative to Gaussian thermal states. The Kurtosis of the homodyne data confirmed these deviations, thus proving the power of QHT to highlight unexpected features of quantum states.

OCIS codes: 270.0270 Quantum optics, 270.6570 Squeezed states

References and links

1. See for example: *Quantum states estimation*, M. G. A. Paris and J. Řeháček Eds., Lect. Not. Phys. **649** (Springer, Heidelberg, 2004).
2. G. Breitenbach, S. Schiller and J. Mlynek "Measurement of the quantum states of squeezed light," Nature, **387**, 471–475 (1997);
3. G. Breitenbach and S. Schiller, "Homodyne tomography of classical and non–classical light," J. Mod. Opt. **44**, 2207–2225 (1997);
4. A. Zavatta, F. Marin and G. Giacomelli, "Quantum-state reconstruction of a squeezed laser field by self-homodyne tomography," Phys. Rev. A **66**, 043805 (2002);
5. G. Mauro D'Ariano, M. De Laurentis, M.G.A. Paris, A. Porzio, and S. Solimeno, "Quantum tomography as a tool for the characterization of optical devices," J. Opt. B **4**, S127–S132 (2002);
6. A. I. Lvovsky, H. Hansen, T. Aichele, O. Benson, J. Mlynek, and S. Schiller, "Quantum State Reconstruction of the Single-Photon Fock State," Phys. Rev. Lett. **87**, 050402 (2001);
7. J. Wenger, R. Tualle-Brouri, and Ph. Grangier, "Non-Gaussian Statistics from Individual Pulses of Squeezed Light," Phys. Rev. Lett. **92**, 153601 (2004);
8. Alessandro Zavatta, Silvia Viciani, and Marco Bellini "Tomographic reconstruction of the single-photon Fock state by high-frequency homodyne detection," Phys. Rev. A **70**, 053821 (2004);
9. G. M. D'Ariano, C. Macchiavello and M. G. A. Paris, "Detection of the density matrix through optical homodyne tomography without filtered back projection," Phys. Rev. A **50**, 4298–4302 (1994).
10. M.J. Collett and C. W. Gardiner,"Squeezing of intracavity and travelling-wave light fields produced in parametric amplification," Phys. Rev. A **30**, 1386–1391 (1984);
11. K. Dechoum, P. D. Drummond, S. Chaturvedi, and M. D. Reid, "Critical fluctuations and entanglement in the nondegenerate parametric oscillator," Phys. Rev. A **70**, 053807 (2004);
12. P. Marian, "Higher-order squeezing and photon statistics for squeezed thermal states," Phys. Rev. A **45**, 2044–2051 (1992);
13. G. M. D'Ariano, M. G. A Paris, and M. F. Sacchi, "Quantum Tomography," Advances in Imaging and Electron Physics **128**, 205–308 (2003).
14. A. Porzio, C. Altucci, M. Autiero, A. Chiummo, C. de Lisio, and S. Solimeno, "Tunable twin beams generated by a type–I LNB OPO," Appl. Phys. B **73**, 763–766, (2001);

#5806 - $15.00 US Received 19 November 2004; revised 27 December 2004; accepted 30 January 2005

15. R.W.P. Drever, J.L. Hall, F.V. Kowalski, J. Hough, G.M. Ford, A.J. Munley, and H. Ward, "Laser phase and frequency stabilization using an optical resonator," Appl. Phys. B **31**, 97–105, (1983);
16. V. D'Auria, P. Aniello, Matteo G.A. Paris, A. Porzio, and S. Solimeno "Quadrature Fourth order moment in an OPO described by time dependent coefficient Langevin equation," *in preparation*

1. Introduction

Quantum homodyne tomography (QHT) is a powerful technique for measuring the state of a quantum field [1]. It is based on balanced homodyne detection of the investigated field (*signal)*. The interference of a strong coherent beam, (*local oscillator* – LO) with the signal at a *beam splitter* (BS) gives a homodyne current proportional to $\eta|z|X(\theta)$ where z is the LO complex amplitude, η the photodetectors' quantum efficiency and $X(\theta) \equiv \frac{1}{2}\left(a_s e^{-i\theta} + a_s^\dagger e^{i\theta}\right)$ the *signal*'s *field-quadrature*. By varying the relative phase θ between the two fields, it is possible to measure $X(\theta)$ over the interval $[0, 2\pi)$. The collection of the outcomes (x, θ) for an adequate number of θ allows the reconstruction of any quantity of interest, including the whole signal's density matrix ρ and, in turn, the Wigner quasi probability distribution.

QHT has been mostly applied to the reconstruction of Gaussian states of the field, as for example coherent and squeezed states [2, 3, 4, 5], or to states intended to be non–Gaussian [6, 7, 8].

The pattern function technique, firstly introduced in [9] provides a method for computing directly from the homodyne data the mean value of interesting quantities. Any operator O, even if not directly detectable as the elements of the density matrix, can be associated to a suitable pattern function $R_\eta[O](x, \theta)$. The corresponding expectation value $\langle O \rangle$ is obtained by averaging the pattern function over homodyne data. The technique automatically compensates for the non–unit efficiency of the detectors η and allows to fully characterize the state without any *a priori* assumption on its statistics.

In this paper we highlight the peculiar characteristic of *pattern function* method of being free of any hypothesis on the state. This is exploited to reveal unexpected deviations from Gaussian state of a vacuum squeezed field due to residual threshold and detuning fluctuations of an OPO source.

We have applied QHT to the output of a pump enhanced degenerate type–I OPO below threshold. In particular, we have investigated these states for different pump power levels with respect to the threshold and cavity escape efficiencies. In the ideal case (single–ended optical cavity, no crystal loss) the output state is a minimum uncertainty one with squeezing in the $\theta = 90^\circ$ quadrature [10]. In practice, for continuous wave (CW) devices, this ideal state can never be generated because of the unavoidable extra–losses of the optical cavity (input mirror residual transmittance and/or crystal absorption). The effect of losses on vacuum squeezed states is both to remove the minimum uncertainty property and to lower the available noise reduction in the squeezed quadrature.

OPO field operators are described by Langevin equations depending linearly on Gaussian noise operators. In recent years some papers have investigated the limits of the linear approximation [11] by concluding that nonlinearity effects are out of reach of the present OPO technology. In fact they can be observed only in the very proximity of the threshold (distance from threshold of the orders of 10^{-6}). The conclusions of Ref. [11] however do not make justice of other mechanisms which could produce some deviation from the Gaussian statistics. We refer here to the unavoidable fluctuations of threshold and detuning phase, which depend on pump, mechanical and thermal fluctuations.

Applying the *pattern function* method to the radiation outing a standard OPO we have reconstructed the photon distributions ρ_{nn} and compared them with those relative to a Gaussian field [12]. Having found some deviations we have analyzed the Kurtosis of the $X(\theta)$ distributions

#5806 - $15.00 US Received 19 November 2004; revised 27 December 2004; accepted 30 January 2005

for each θ finding evidence of non Gaussian features. This provides evidence of the ability of the above QHT method to recover the state details.

The paper is structured as follows. Section 2 outlines data analysis strategy and gives a general glance to *pattern function* QHT. In section 3 a description of the experiment is given while section 4 discusses the experimental results. Eventually, conclusions are drawn in section 5.

2. Data analysis

The *pattern function* QHT provides the complete quantum characterization of an optical signal by average a suitable function over homodyne detection. Scanning the LO phase over a 2π interval, the expectation value of any observable O is obtained as [13]:

$$\langle O\rangle = Tr[\rho\ O] = \int_0^{2\pi}\frac{d\theta}{2\pi}\int_{-\infty}^{\infty} dx\ p_\eta(x,\theta)\ R_\eta[O](x,\theta) \tag{1}$$

with $p_\eta(x,\theta)$ the distribution of the outcomes x for the quadrature $X(\theta)$, ρ the system density matrix and η the detector efficiency. The pattern function $R_\eta[O](x,\theta)$ is:

$$R_\eta[O](x,\theta) = Tr\left[O\ K_\eta(X(\theta)-x)\right]$$

with

$$K_\eta(x) = \frac{1}{2}\Re\left[\int_0^{+\infty} k\ dk\ e^{\frac{1-\eta}{8\eta}k^2+ikx}\right].$$

If $R_\eta[O](x,\theta)$ satisfies the hypothesis of the central limit theorem, the statistical error on the tomographic measurement is given by

$$\delta O = \frac{1}{\sqrt{N}}\left\{\overline{\Delta R_\eta^2[O]}\right\}^{1/2}$$

with N the number of data and $\overline{\Delta R_\eta^2[O]}$ the variance of $R_\eta[O]$ over data.

In particular, the photon number distribution can be reconstructed from the diagonal elements of the density matrix $\rho_{nn} = \langle n|\rho|n\rangle$ the pattern function for the projectors being

$$R_\eta[|n\rangle\langle n|](x,\theta) = \int_{-\infty}^{+\infty} dk\,|k|e^{\frac{1-2\eta}{2\eta}k^2-i2kx}L_n(k^2)\ , \tag{2}$$

with $L_n(x)$ the n–th Laguerre polynomials. Remarkably, the variances of the field quadrature $\Delta X(\theta)$ themselves can be reconstructed using the homodyne data. We have

$$R_\eta[\Delta X^2(\psi)](x,\theta) = R_\eta[X^2(\psi)](x,\theta) - \overline{R_\eta[X(\psi)]}^2 \tag{3}$$

with

$$\begin{aligned} R_\eta[X^2(\psi)](x,\theta) &= \frac{1}{4}\left\{1+(4x^2-\frac{1}{\eta})\left[4\cos^2(\theta-\psi)-1\right]\right\} \\ R_\eta[X(\psi)](x,\theta) &= 2x\cos(\theta-\psi) \end{aligned}$$

The experimental apparatus enters QHT procedure only through the calibration of the data with respect to the measured shot noise. We stress that *pattern function* allows to recover the "true" properties of the state without making any hypothesis on it. In this way, it can be used for investigating some features of a nonclassical light source. For example, a departure of the QHT reconstructed ρ_{nn} from the ones predicted for a Gaussian state, suggests the limits of an OPO model based on constant coefficient Langevin equations.

#5806 - $15.00 US Received 19 November 2004; revised 27 December 2004; accepted 30 January 2005

An OPO with linearized and time independent coefficient Langevin equation, generates a Gaussian *squeezed thermal vacuum (*STV) with density matrix

$$\rho = S(\zeta)\nu S^{\dagger}(\zeta)$$

being $S(\zeta) = \exp\left\{\frac{1}{2}\zeta^2 a^{\dagger 2} - \frac{1}{2}\zeta^{*2}a^2\right\}$ the squeezing operator ($\zeta = re^{i\psi}$ squeezing parameter), and $\nu = (n_t+1)^{-1}\left[n_t/(n_t+1)\right]^{a^{\dagger}a}$ a thermal state density matrix with n_t average photon number. n_t and r depend on the OPO coupling efficiency $\eta_{out} = \frac{\gamma_s}{\kappa_s}$ ($\kappa_s = \gamma_s + \varkappa_s$ cavity damping including output mirror γ_s and extra–losses $\varkappa_s$) and distance from the threshold $\mathscr{E} = \frac{P}{P_{th}}$ (P pump power, P_{th} threshold power). For $\eta_{out} = 1$, $n_t = 0$ the state is the squeezed vacuum described in [10]. For $\eta_{out} < 1$ the state is no more a pure neither a minimum uncertainty one. Given η_{out}, $\Delta X(\theta)$ shows an oscillatory dependence on θ with the maximum ($\theta = 0$) and minimum ($\theta = \pi/2$) respectively increasing and decreasing as $\mathscr{E} \to 1$.

Assuming that the signal is a STV and using QHT reconstruction of squeezed (ΔY) and anti-squeezed (ΔX) quadrature variances (see Eq. 3) one can recover n_t and r from the relations

$$n_t = 4\,\Delta X\,\Delta Y - 1, \qquad r = \frac{1}{2}\ln\frac{\Delta Y}{\Delta X}$$

Then, the photon number distribution follows from Eq. 23 in ref. [12]:

$$p_n = \frac{C^n}{A^{n+\frac{1}{2}}} P_n\left(\frac{B}{C}\right) \tag{4}$$

being $P_n(x)$ the n-th Legendre function of the first kind and

$$\begin{aligned} A &= (1+n_t)^2 - (2n_t+1)\sinh^2 r \\ B &= n_t(1+n_t) \\ C &= \sqrt{n_t^2(1+n_t)^2 - (2n_t+1)^2\sinh^2 r\cosh^2 r} \end{aligned}$$

A difference between ρ_{nn} and p_n suggests a deviation of the actual state from the expected STV.

3. Experimental set-up

The experimental setup, described in more details in Ref. [14], basically consists of a type–I $LiNbO_3$:MgO OPO, the homodyne detector and a data acquisition board (see Fig.1).

The second harmonic beam (@532nm) of a frequency-doubled dual wavelength continuous wave Nd:YAG laser (Lightwave model 142, P_g=145 mW @532 nm and P_{IR}=45 mW @1064 nm, shot–noise–limited above 2.5 MHz, 5 dB above the shot noise at 2 MHz) is used for pumping the OPO. The OPO cavity is locked to the pump beam by Pound-Drever technique [15]. Degeneracy is achieved by finely tuning the non–linear crystal temperature (residual fluctuations $\leq$1.mK for longer than one hour).

Tomographic data have been acquired by changing the OPO cavity end mirror resulting in two different value for the cavity escape efficiency η_{out}.

The OPO output goes to a homodyne detector with a total detection efficiency $\eta = 0.88 \pm 0.02$. Mode matching at the BS has been accomplished by spatially filtering the LO beam by a mode cleaner cavity (MC), similar to the OPO one ($\Delta l = |l_{OPO} - l_{MC}| < 0.1$ mm). An optical delay line with a resolution of 10 μm is used for matching the two optical paths, while two half-waves-plates guarantee polarization matching. Visibilities of 0.97 ± 0.02 have been repeatedly obtained.

#5806 - $15.00 US Received 19 November 2004; revised 27 December 2004; accepted 30 January 2005

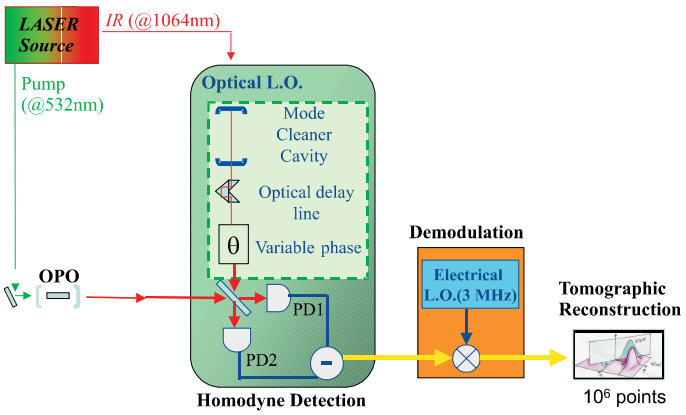

Fig. 1. Schematic of the experimental setup. It essentially consists of two main parts: I – the OPO source (described into details in Ref. [14]) II – detection and acquisition bench made of a homodyne detector, a demodulation module and a PCI acquisition card (14 bits resolution).

Each photodiode (Epitaxx ETX300) is matched to a low–noise trans–impedance AC ($>$ few kHz) amplifiers based on CLC425. The difference photocurrent is further amplified by a low noise high gain amplifier (Miteq AU1442 G=34dB, noise figure 1.2).

Acquisition is triggered by a linear ramp applied to the PZT, that drives θ. The ramp is adjusted to obtain a 2π variation in an acquisition window.

Tomographic data are acquired by sampling the difference photocurrent. To avoid bad influence from the laser low frequency noise, data sampling is moved away from the optical carrier frequency ω_{IR} by mixing the homodyne current with a sinusoidal signal of frequency Ω. Tomographic measurements are performed at $\Omega = 3\,\mathrm{MHz}$ well inside the cavity bandwidth ($\Delta\nu = 15$ and $18\,\mathrm{MHz}$ for $\eta_{out} = 0.4$ and 0.5 respectively). The resulting current, filtered by a cascade of low–pass filters with total bandwidth $B \simeq 1\,\mathrm{MHz}$, is eventually sampled by a digital acquisition PC based module (Gage 14100) able to acquire up to 1M–points per run with 14 bits resolution.

The sampling rate ν has been fixed to 5 Msamples/s for experimental convenience. We note that a ratio $\frac{B}{\nu} < 1$ reduces the number of totally uncorrelated samples. In this way the number of effective samples is given by $N_{eff} = N \times \frac{B}{\nu}$. Being the measured process stationary the filtering-sampling procedure does not alter the statistics of the outcomes. Our sampling conditions are similar to the ones utilized in Ref. [2] while they used a ten times narrower filter. So doing we have chosen to privilege the effective number of samples with respect to a better defined spectral selection.

Calibration with respect to the noise of the coherent vacuum state is obtained by acquiring a set of data by obscuring the signal while scanning the LO phase θ. The total electronic noise power has been measured to be 15 dBm below the shot–noise level.

4. Experimental results

In order to assess the role of threshold fluctuations we have reconstructed the states for different values of η_{out} and $\mathscr{E}$.

The first set of data is relative to $\eta_{out} = 0.4$ and $\mathscr{E} = 0.5$, 0.8 and 0.95. The threshold has been directly measured at the end of the tomographic acquisition. For each value of $\mathscr{E}$ we have acquired typically 5 homodyne traces and recovered for each ρ_{nn} (up to $n = 6$, see Eq. (2)) and the quadrature variances (ΔX, ΔY) normalized to the shot–noise.

#5806 - $15.00 US Received 19 November 2004; revised 27 December 2004; accepted 30 January 2005

The reconstructed ΔX and ΔY have been used for computing the photon number probability p_n by means of Eq.4 under the assumption of Gaussian state. Then, p_n have been compared to ρ_{nn}.

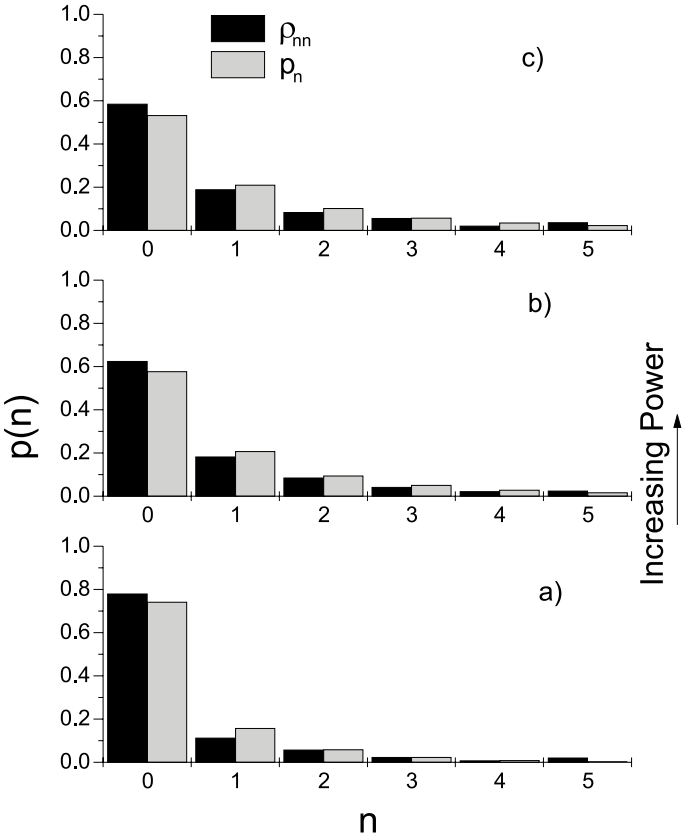

Fig. 2. Photon number distribution for $\mathscr{E} = \frac{P}{P_{th}} = 0.5$ (a), 0.8 (b) and 0.95 (c) as recovered by pattern function tomography (ρ_{nn} – black columns) and in the Gaussian state hypothesis (p_n – grey columns). The two determinations are different with a deviation increasing with pump power. Confidence intervals (not shown) are much smaller that the difference between the two determinations.

In Fig. (2) we report ρ_{nn} and p_n for $\mathscr{E} = 0.5$ (lower plot), 0.8 and 0.95 (upper plot). As it can be seen the two determinations are sensibly different, their difference being larger the closer the OPO is to the threshold. For $\mathscr{E} = 0.5$ (lower plot) $\rho_{00} = 0.780$ and $p_0 = 0.743$ (¡ 3% difference), while for $\mathscr{E} = 0.95$ (upper plot) $\rho_{00} = 0.585$ and $p_0 = 0.533$ (10% difference). For $\mathscr{E} = 0.8$ (middle plot) is 8%.

This behavior has been confirmed by a second set of measurements performed with higher coupling efficiency ($\eta_{out} = 0.5$). In this case we have acquired data for $\mathscr{E} = 0.5$, 0.60, 0.65, 0.70, and 0.8. Similarly to the previous case, the relative deviation between ρ_{00} and p_0 increases with $\mathscr{E}$, while for given $\mathscr{E}$ it is lower for higher η_{out}. The maximum deviation is less than 6% for $\mathscr{E} = 0.8$. In Fig. 3 we report the relative deviation between ρ_{00} and p_o for both coupling efficiencies.

In order to understand the origin of these differences we have tested the Gaussian character of the state by analyzing the data statistics at a fixed θ. For a Gaussian state, in fact, the Wigner

#5806 - $15.00 US Received 19 November 2004; revised 27 December 2004; accepted 30 January 2005

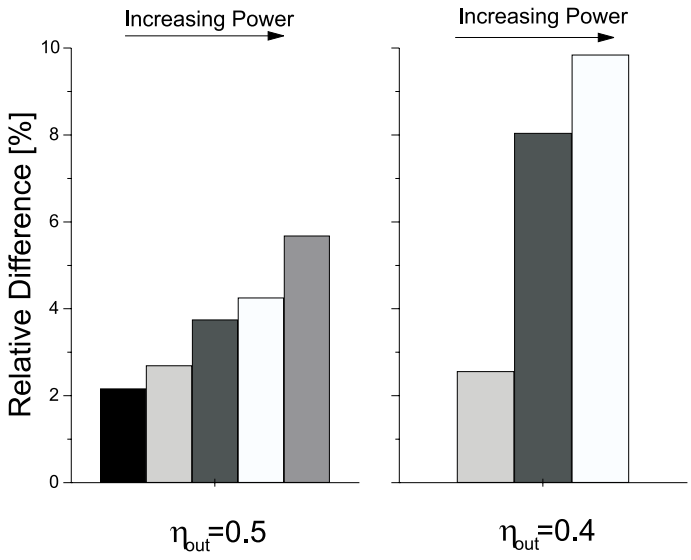

Fig. 3. Relative difference between the two experimental determinations of ρ_{00} (by pattern function tomography) and p_0 (Gaussian hyphotesis). The reported deviations correspond to $\mathscr{E} = 0.5$, 0.6, 0.65, 0.7, and 0.8 ($\eta_{out} = 0.5$), and $\mathscr{E} = 0.5$, 0.8 and 0.95 ($\eta_{out} = 0.4$).

function is Gaussian and so is the marginal distribution $p(x,\theta)$ at fixed θ. Any deviation of $p(x,\theta)$ from a Gaussian is an indication of the deviation of the state itself. The deviation of a statistical distribution from a Gaussian can be evaluated by means of the Kurtosis

$$K = \frac{1}{N}\sum_{i=1}^{N}\frac{(x_i - \bar{x})^4}{\sigma^4} - 3$$

which vanishes in the Gaussian case.

Each data set refers to a LO phase θ spanning between 0 and 2π corresponding to 10^6 points acquired in 200 ms. In order to test the statistics at a fixed θ_n we have divided the tomographic set in 100 phase bins (10000 data each, lasting 2 ms). The histogram of these data describes $p(x,\theta_n)$ for $X(\theta_n)$. We found a clear deviation from a Gaussian particularly for the anti–squeezed quadrature, increasing as the threshold is approached. In Fig. 4 we report the $p(x,\theta_n)$ variance and Kurtosis versus the phase BIN. For low pump level the Kurtosis keeps below 0.15 for any θ_n while for powers close to the threshold (upper plot) K reaches $0.4 \div 0.5$ in correspondence of the two variance maxima. In all the acquisitions K is practically 0 in correspondence of variance minima.

We note that at $\mathscr{E} = 0.8$ for $\eta_{out} = 0.5$ the deviations between ρ_{nn} and p_n are smaller than those observed for $\eta_{out} = 0.4$. This could indicate a less critical influence of $\mathscr{E}$ as the coupling efficiency is enhanced. Nevertheless, the Kurtosis in the two cases are equal within their error.

We note that K for calibration data is zero within $5 * 10^{-3}$, thus ensuring no spurious effects of the detection apparatus on the observed distributions. Moreover, the correct functioning of the homodyne set-up (optics + photodiodes + electronics) has been tested [5] in the tomographic reconstruction of few photon coherent states.

This behavior can be reconducted to residual fluctuations of the OPO parameters. In the case of a single–ended cavity the field inside the OPO, a_s satisfies an equation of the form

$$\frac{d}{dt}\hat{a}_s = [\chi + \delta\chi(t)]\,\hat{a}^\dagger - [\gamma_s + i\Delta(t)]\,\hat{a}_s + \sqrt{2\gamma_s}\hat{a}^{in}$$

#5806 - $15.00 US Received 19 November 2004; revised 27 December 2004; accepted 30 January 2005

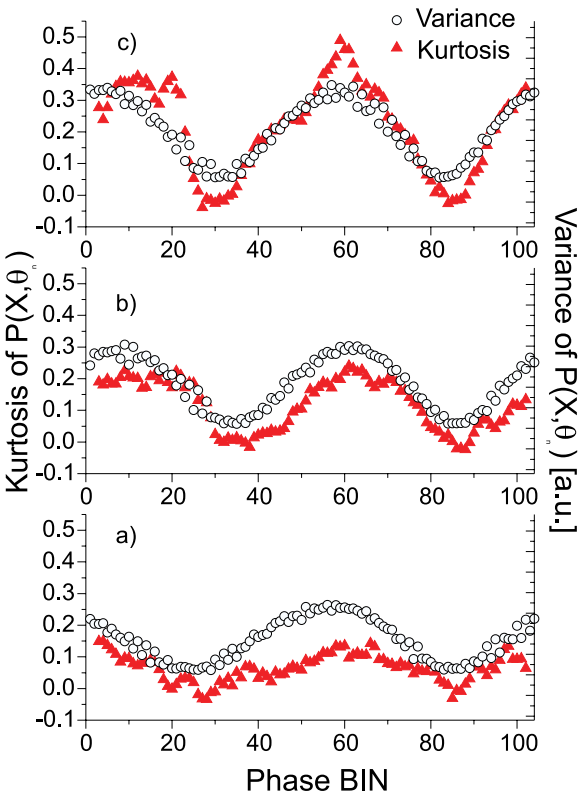

Fig. 4. Kurtosis of $p(x,\theta_n)$ (red triangles) for three homodyne data sets: $\mathscr{E} = \frac{P}{P_{th}} = 0.5$ (a), 0.8 (b) and 0.95 (c). Empty circles indicate the variance (given in a.u.) for the same θ_n. The phase BIN at which the variance and the Kurtosis are maximum coincides. The Kurtosis goes practically to 0 in correspondance of variance minima. The highest Kurtosis is ≈ 0.5 for $\mathscr{E} = 0.95$. In this case the relative deviation between ρ_{00} and p_0 (see text for details) reaches 10%. It is worth noting that it has been observed a maximum noise reduction of 2.4 dB.

with fluctuating detuning $\Delta(t)$ and non linear coupling coefficient $\chi + \delta\chi(t)$ with

$$\delta\chi(t) = \chi\left(\frac{\delta|a^{\ell}|}{|a^{\ell}|} - \frac{\delta T^2}{\Delta T^2} - \frac{\Delta^2}{\gamma^2}\right)$$

depending on the pump $\delta|a^{\ell}|$, temperature δT and detuning Δ residual variations. Laser pumps may exhibit intensity fluctuations of $\sim 1\%$, while a Drever-Pound system stabilizes the cavity with a residual detuning of $\sim 10^{-2} \div 10^{-3}\gamma_s$.

Ignoring these fluctuations $\hat{a}_s$ inherits the Gaussian statistics of $\hat{a}^{in}$ thus giving rise to a squeezed vacuum [10]. Switching on $\delta\chi(t)$ and $\Delta(t)$ $\hat{a}_s$ begins to deviate from the Gaussian state the more the greater $\overline{\delta\chi^2}$ and $\overline{\Delta^2}$ are [16]. These results can be generalized to a double–ended cavity.

5. Conclusions

In this paper we have examined the accuracy of quantum homodyne tomography (QHT) technique based on *pattern functions*, as applied to the vacuum squeezed field generated by an

#5806 - $15.00 US Received 19 November 2004; revised 27 December 2004; accepted 30 January 2005

OPO below threshold. We show that this method is able to detect small state deviations from a Gaussian statistics, due to the residual fluctuations of threshold and detuning.

Operating the OPO away and close to the threshold, we have obtained a set of density matrix elements deviating in a more or less pronounced way from those of a vacuum squeezed thermal state. These deviations have been confirmed by directly analyzing the distribution functions of the quadratures $X(\theta)$ for 100 values of θ. Plotting the Kurtosis (K) of each distribution as a function of θ for different distances from the threshold we found that K is minimum(maximum) for the squeezed (anti–squeezed) quadrature. In general K_{max} decreases by moving away from the threshold.

We conclude that QHT based on pattern function is an effective method for characterizing quantum signals and assessing the correct operation of non classical light sources.

#5806 - $15.00 US Received 19 November 2004; revised 27 December 2004; accepted 30 January 2005